

Superconducting micro-resonator arrays with ideal frequency spacing

Cite as: Appl. Phys. Lett. **111**, 252601 (2017); <https://doi.org/10.1063/1.5016190>

Submitted: 16 November 2017 . Accepted: 06 December 2017 . Published Online: 20 December 2017

X. Liu, W. Guo, Y. Wang, M. Dai, L. F. Wei, B. Dober, C. M. McKenney, G. C. Hilton, J. Hubmayr, J. E. Austermann, J. N. Ullom, J. Gao, and M. R. Visser



View Online



Export Citation



CrossMark

ARTICLES YOU MAY BE INTERESTED IN

[Cryogenic LED pixel-to-frequency mapper for kinetic inductance detector arrays](#)
Journal of Applied Physics **122**, 034502 (2017); <https://doi.org/10.1063/1.4994170>

[Counting near infrared photons with microwave kinetic inductance detectors](#)
Applied Physics Letters **110**, 212601 (2017); <https://doi.org/10.1063/1.4984134>

[Photon-noise limited sensitivity in titanium nitride kinetic inductance detectors](#)
Applied Physics Letters **106**, 073505 (2015); <https://doi.org/10.1063/1.4913418>

Lock-in Amplifiers
up to 600 MHz



Superconducting micro-resonator arrays with ideal frequency spacing

X. Liu,¹ W. Guo,^{2,3,a)} Y. Wang,¹ M. Dai,³ L. F. Wei,^{1,3,4} B. Dober,² C. M. McKenney,²
 G. C. Hilton,² J. Hubmayr,² J. E. Austermann,² J. N. Ullom,² J. Gao,² and M. R. Vissers²

¹Quantum Optoelectronics Laboratory, School of Physical Science and Technology, Southwest Jiaotong University, Chengdu 610031, China

²National Institute of Standards and Technology, Boulder, Colorado 80305, USA

³Information Quantum Technology Laboratory, School of Information Science and Technology, Southwest Jiaotong University, Chengdu 610031, China

⁴State Key Laboratory of Optoelectronic Materials and Technologies, School of Physics, Sun Yat-Sen University, Guangzhou 510275, China

(Received 16 November 2017; accepted 6 December 2017; published online 20 December 2017)

We present a wafer trimming technique for producing superconducting micro-resonator arrays with highly uniform frequency spacing. With the light-emitting diode mapper technique demonstrated previously, we first map the measured resonance frequencies to the physical resonators. Then, we fine-tune each resonator's frequency by lithographically trimming a small length, calculated from the deviation of the measured frequency from its design value, from the interdigitated capacitor. We demonstrate this technique on a 127-resonator array made from titanium-nitride and show that the uniformity of frequency spacing is greatly improved. The array yield in terms of frequency collisions improves from 84% to 97%, while the quality factors and noise properties are unaffected. The wafer trimming technique provides an easy-to-implement tool to improve the yield and multiplexing density of large resonator arrays, which is important for various applications in photon detection and quantum computing. <https://doi.org/10.1063/1.5016190>

Superconducting micro-resonators are important for many applications such as photon detection,¹ quantum-limited amplifiers,² readout of superconducting qubits,³ and readout of nanomechanical resonators.⁴ They are of particular interest for superconducting detector applications because they are simple to fabricate and a large array of detectors can be read out through microwave frequency-domain multiplexing, which significantly reduces the complexity and cost of cryogenic wirings and readout electronics. For example, microwave kinetic inductance detectors (MKIDs)^{1,5,6} are low-temperature detectors based on high-quality factor (high- Q) superconducting resonators.⁷ A large MKID array with thousands of resonators (pixels) can be fabricated with a small number of photolithography steps and read out with only a pair of coaxial cables into the cryostat. After over a decade of development, MKIDs are now used in both astronomical instruments^{8–11} and non-astronomical applications.^{12–14}

The pixel counts of large MKID arrays in major MKID instruments deployed and in development are growing rapidly, from hundreds^{15–17} to thousands^{18–21} of pixels per wafer. As the array size and multiplexing density increase, resonator frequency collisions have become a serious problem that limits the array yield. The resonance frequencies are inevitably shifted from their design values due to various factors, such as non-uniformity in the superconducting critical temperature (T_c), film thickness, and over-etch depth across the wafer. When two resonators are too close to each other in frequency space, referred to as a frequency collision, they cannot be read out properly due to cross-talk, thus reducing the effective array yield. Here, the yield is defined as the number of useful non-colliding pixels over the total number of resonators. This problem becomes more severe in larger

arrays because more resonators must be placed in a given frequency bandwidth, requiring smaller spacing between adjacent resonance frequencies, resulting in more unwanted frequency collisions.

There are several approaches to reduce frequency collisions to improve the yield for large MKID arrays. The first approach is to increase the quality factor Q of the resonators. However, in many applications, the detector bandwidth and optical loading conditions limit the highest Q to be less than $\sim 50\,000$. Another approach is to improve the fabrication process in order to achieve better wafer uniformity. For example, at NIST, we have developed proximity-coupled TiN/Ti/TiN trilayer and multilayer films for the next generation balloon-borne large aperture submillimeter telescope (BLAST-TNG), which have greatly reduced the T_c non-uniformity from over 20% to less than 2% across a 76.2 mm wafer^{22,23} as compared to sub-stoichiometric TiN films.²⁴ As the size of the array and the required multiplexing density continue to grow, it becomes more and more challenging to reduce frequency collisions through further improvement in the film uniformity.

In this letter, we propose an alternative easy-to-implement technique based on two successive rounds of design, fabrication, and measurement to produce a final resonator array with ideal frequency spacing and an extremely low frequency collision rate. In the second round, the resonance frequencies are re-tuned by lithographically trimming the interdigitated capacitor (IDC) of each resonator, using the measured resonance frequency information from the first round. We demonstrate this technique on a 127-resonator array from a TiN/Ti/TiN multilayer film and show that the array yield improves from 84% to 97%, while the resonator quality factors and noise properties remain unaffected.

In this work, we study lumped-element kinetic inductance detectors (LEKIDs)⁵ consisting of an inductor and an

^{a)}Author to whom correspondence should be addressed: weijie.guo@nist.gov

IDC. In our LEKID array, all the resonators are designed to have the same inductor, and the unique frequency of each resonator is defined by varying the number of IDC fingers. The trimming technique consists of 6 steps which involve two rounds of design, fabrication, and measurement. Figure 1(a) shows a flow chart of the steps which are explained below:

Step 1: Initial design of the MKID array. Assume that we want to design an array of N resonators with design frequencies of $f_{\text{des},i}$ ($i = 1, 2, \dots, N$). The set $\{f_{\text{des},i}\}$ usually forms a frequency comb which fits within a certain readout bandwidth. The desired number of IDC fingers of each resonator $N_{\text{IDC},i}$ (ranging between 59 and 99 for our design) is calculated from the relation $f_{\text{des},i} = 1 / \left(2\pi \sqrt{L\tilde{C}N_{\text{IDC},i}} \right)$,

where the capacitance per finger (1200 μm) $\tilde{C} = 66$ fF and the total inductance $L = 6.95$ nH are derived from electromagnetic simulations using empirical material parameters obtained from previous experiments. In this initial design step, we have ignored any wafer non-uniformity and assumed common L and \tilde{C} among all the resonators.

Step 2: First fabrication. In this step, the wafer is patterned into an array of resonators with the design number of IDC fingers $N_{\text{IDC},i}$.

Step 3: Frequency measurement and LED mapping. It is straightforward to measure the transmission S_{21} of the entire array which contains all the resonances using a vector network analyzer (VNA). However, it is difficult to correctly

correspond each resonance to its physical resonator on the wafer because the resonances are shifted from their design values due to wafer non-uniformity. In this step, we use the LED wafer mapping tool that we have previously developed especially for this purpose²⁶ to establish the correspondence between the measured frequency $f_{\text{mea},i}$ and the number of fingers $N_{\text{IDC},i}$ of the i -th resonator on the wafer.

Step 4: Array re-design. To account for the deviation of $f_{\text{mea},i}$ from $f_{\text{des},i}$ due to wafer non-uniformity, we set up a

new model $f_{\text{mea},i} = 1 / \left(2\pi \sqrt{L_i \tilde{C}_i N_{\text{IDC},i}} \right)$, where L_i and \tilde{C}_i are introduced to account for the local variations of inductance and capacitance at the location of the i -th resonator. By analyzing the $f_{\text{mea},i}$ vs. $N_{\text{IDC},i}$ data obtained from Step 3, we retrieve the local $L_i \tilde{C}_i$ product of each resonator. We then set up a new frequency comb $\{f_{\text{des},i}^*\}$ as our new design frequencies. We require that $f_{\text{des},i}^* \geq f_{\text{mea},i}$ because in the next step, we will etch off a small portion from the original IDC fingers. Calculated from $f_{\text{des},i}^* = 1 / \left(2\pi \sqrt{L_i \tilde{C}_i N_{\text{IDC},i}^*} \right)$

using the derived $L_i \tilde{C}_i$ values, the i -th resonator is re-designed to have a new number of IDC fingers $N_{\text{IDC},i}^*$ ($\leq N_{\text{IDC},i}$).

Step 5: IDC trimming. In this step, the wafer is sent back to the clean room and a small portion of each IDC is trimmed off using lithographical tools and reactive ion etching which reduces the number of IDC fingers from $N_{\text{IDC},i}$ to $N_{\text{IDC},i}^*$.

Step 6: Frequency re-measurement of the trimmed array. In this step, we repeat the VNA sweep and LED mapping procedures in Step 3 to obtain the new resonance frequencies $\{f_{\text{mea},i}^*\}$. Comparison and statistics are carried out on both $f_{\text{mea},i}^*$ and $f_{\text{des},i}^*$ to evaluate the effect of the array trimming technique.

To demonstrate our array trimming technique, we made a 127-pixel hexagonal close-packed LEKID array from a 60 nm thick multilayer TiN/Ti/TiN film ($T_c \approx 1.6$ K) on a 76.2 mm intrinsic Si wafer. Both the pixel design and array format are identical to BLAST-TNG²⁵ in the 500 μm band. Each pixel consists of orthogonal TiN absorbers attached to a pair of IDC [Fig. 1(b)]. In this letter, we study only the 127 X-pol resonators.

In the initial design step (Step 1), the design resonance frequencies are in a geometric series as $f_{\text{des},i} = 750 \text{ MHz} \times 1.002^{i-1}$, where $i = 1, \dots, 127$ is the resonator index along the meandering feedline on the wafer. The coupling quality factor is designed to be $Q_c \approx 30\,000$, which will yield a total quality factor $Q \approx 20\,000$ under optical loading (quality factor reduced under background loading due to Cooper pair breaking). Both Q and Q_c values are taken from the BLAST-TNG 500 μm array design.²⁵

In the first fabrication step (Step 2), we patterned the wafer using a semi-automated “tiling and trimming” technique developed for BLAST-TNG arrays with a stepper tool.²⁷ In this technique, a mask of the standard pixel tile [Fig. 1(b)] containing the common inductor part and a full IDC with 176 fingers is repeatedly exposed onto the wafer at the desired pixel positions. A second set of IDC trimming masks [dark blue area in Fig. 1(c)] is used to cut each

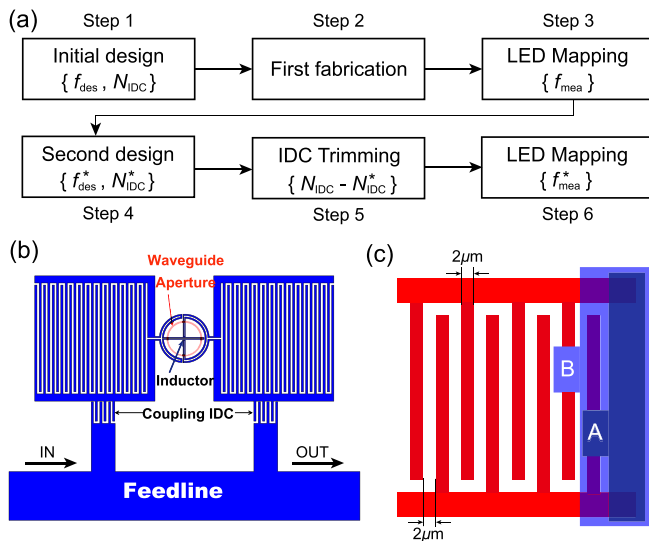


FIG. 1. (a) A flow chart of the trimming technique consisting of 6 steps with two rounds of design, fabrication, and measurement. (b) Schematic drawing (not to scale) of the MKID single-pixel design for BLAST-TNG.²⁵ There are two lumped-element MKIDs within a pixel, and the two inductors are orthogonally aligned to achieve dual-polarization-sensitivity. The red circle shows the waveguide aperture where the inductive absorbers are illuminated by millimeter-wave radiation. (c) Schematic illustration of the IDC trimming process. The red area represents the IDC fingers (2 μm finger/gap width). The dark/light blue areas represent the areas where IDC fingers are etched off. In the first fabrication step (Step 2 in the flow chart), the first finger from the right was cut at position “A,” leaving a gap there (dark blue area). In the IDC trimming step (Step 5), the first finger from the right is entirely etched off and the second finger from the right was cut at position “B” (light blue area). The total number of IDC fingers is reduced, and the frequency is tuned upwards.

resonator's IDC fingers at the desired position [position "A" in Fig. 1(c)] to create the designed frequency comb. This fabrication technique limits the number of stepper masks, ensures high quality and uniformity in the stepper lithography because all pixels are patterned from the same standard pixel mask, and provides considerable flexibility in resonator frequency definition and array layout.

After the wafer is made, we cooled it down along with the LED-mapper setup (Step 3) in a dilution refrigerator. We measured the transmission S_{21} of the MKID array at the base temperature of 40 mK using a VNA, and all the resonances were matched to their physical pixel on the wafer using the LED-mapper tool. As shown by the red curve in Fig. 2, 127 resonance dips are clearly observed in the frequency range spanning from 700 MHz to 930 MHz. The local $L_i\bar{C}_i$ values for each resonator were determined after the LED mapping process.

In the re-design step (Step 4), in order to correct the effect of wafer non-uniformity, we selected a new set of design frequencies $f_{des,i}^* = 739 \text{ MHz} \times 1.002^{i-1}$ and designed a new set of $N_{IDC,i}^*$ based on the local $L_i\bar{C}_i$ values obtained in Step 3.

In the next re-fabrication step (Step 5), a small portion of the IDC finger ($N_{IDC,i} - N_{IDC,i}^*$) was lithographically patterned and removed [blue area in Fig. 1(c)] for resonators that require frequency trimming. While it is possible to use the stepper tool and the same IDC trimming mask again to cut the IDC fingers, we used a maskless aligner (MLA) tool which is more convenient and can also be used for non-standard wafer size. It directly exposes a whole-wafer pattern from a computer file containing all areas to be etched off onto the wafer by laser scanning without using a chrome mask. The pattern file was generated by our homemade program which automatically draws the 127 patches [blue area in Fig. 1(c)] at the calculated positions. Although the lithography resolution of the MLA ($\sim 1 \mu\text{m}$) is poorer than the stepper (sub-micrometer), it is adequate for our purpose, and the lithographical error has a negligible effect on the resonance frequency.

After IDC trimming, we measured the MKID wafer at 40 mK again, and S_{21} is shown by the blue curve in Fig. 2.

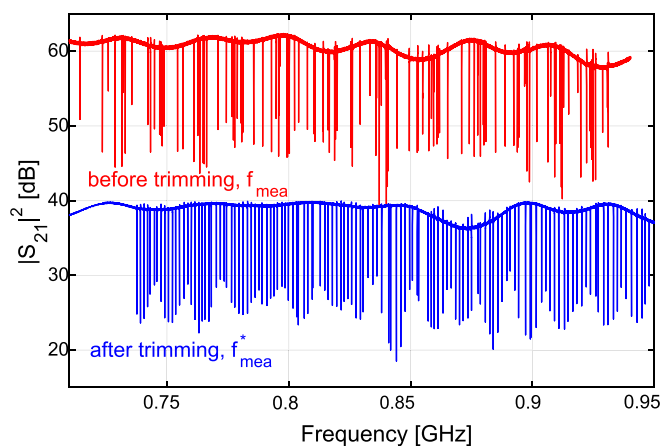


FIG. 2. A comparison of S_{21} (including cable loss and amplifier gain) for the MKID array before (red) and after (blue) the trimming process. The red curve is moved up by 20 dB for clarity. Note that the resonance depths are unchanged after trimming, suggesting that the quality factors are unchanged.

One can see that the resonances are globally shifted up by about 20 MHz since we have reduced the number of IDC fingers for most resonators. It is obvious that the uniformity of the frequency spacing after trimming is greatly improved.

Figure 3(a) shows the design and measured frequency before and after trimming. The fractional frequency deviation $\delta = (f_{mea} - f_{des})/f_{des}$, which reveals the quantitative agreement between the measured and design frequencies, is plotted in Fig. 3(b). Before trimming, f_{mea} exhibits an obvious periodic deviation from f_{des} as shown in both Figs. 3(a) and 3(b). As discussed in our previous paper,²⁶ this is caused by a radial non-uniformity of T_c across the wafer in multilayer TiN/Ti/TiN films. Resonators near the turns of the meandering feedline are in general located on the outer ring of the wafer where T_c is lower and kinetic inductance is higher, leading to the larger negative deviation of the resonance frequency. On average, f_{mea} is lower by a factor of $\sim 2.4 \times 10^{-2}$ than its design value f_{des} , which may be attributed to the inaccurate L and C values used in the initial design and the wafer non-uniformity. It is clear that the measured frequency is much closer to the design frequency after the trimming process, as shown in Fig. 3(b). The maximum deviation $|\delta|_{max}$ is only 4.5×10^{-3} which is significantly smaller than that before trimming. We notice that all the measured frequencies shifted down by $\sim 2 \times 10^{-3}$ from the design frequencies. As a reference, the 76th resonator is untrimmed during the re-fabrication process ($N_{IDC,76} = N_{IDC,76}^*$), but its frequency also shifted down by 2×10^{-3} like other trimmed resonators. This suggests that the global shift is a systematic effect (such as surface oxidation), which is not associated with the array trimming process. Taking $Q = 20\,000$, the 5-linewidth frequency collision criterion (the spacing between adjacent resonances is smaller than $5f/Q$) excludes 20 (or 16%) resonators before trimming and only 4 (or 3%) resonators after trimming. Therefore, the array yield is significantly improved, from 84% to 97%.

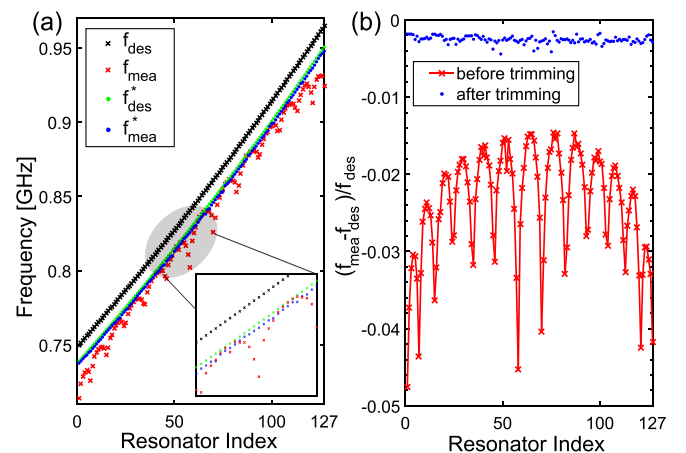


FIG. 3. (a) Design and measured resonance frequency vs. resonator (pixel) index. The black cross and red cross represent the design frequency (f_{des}) and the corresponding measured frequency (f_{mea}) before trimming. The green point and blue point are the design frequency f_{des}^* and measured frequency f_{mea}^* after trimming. Compared to the data before trimming, the periodic deviation vanishes and the deviation of f_{mea}^* from f_{des}^* is too small to distinguish in (a). (b) The fractional frequency deviation vs. resonator index, which shows that the trimming technique significantly reduces the deviation between the design and measured frequency.

Figure 4 compares the distribution of fractional frequency spacing for the MKID array before and after the trimming process. Here, the fractional frequency spacing is calculated from $\delta f/f = (f_{\text{mea},n+1} - f_{\text{mea},n})/f_{\text{mea},n}$, $n=1, \dots, 126$. Before trimming, $\delta f/f$ shows larger scatter from 1×10^{-5} to 1.3×10^{-2} , while the design fractional spacing is 2×10^{-3} . The scatter is greatly reduced after the trimming process. The histogram in Fig. 4(b) fits well to a Gaussian distribution, which allows us to predict the ultimate array yield from the formula derived in the [supplementary material](#)

$$P_0 = \left\{ \prod_{n=1}^{n=\infty} \left[1 - \frac{\text{Erf}\left(\frac{n\Delta}{\sqrt{2}\sigma} + \frac{\chi w}{\sqrt{2}\sigma}\right) - \text{Erf}\left(\frac{n\Delta}{\sqrt{2}\sigma} - \frac{\chi w}{\sqrt{2}\sigma}\right)}{2} \right] \right\}^2, \quad (1)$$

where P_0 is the probability for a resonator to survive collisions with all the other resonators, $w = 1/Q$ is the normalized resonator linewidth, Δ is the designed fractional frequency spacing, and σ is the standard deviation of the Gaussian distribution. Assuming 5-linewidth exclusion, $\chi = 5$, the yield of a MKID array with 1000 resonators distributed in an octave bandwidth is predicted to be 81%. This yield and the multiplexing density are desirable for many MKID instruments and their readout electronics.

Last, we have also verified that the quality factor and noise of the resonators remain unchanged before and after the trimming process. Therefore, the detector performance is not affected. In conclusion, we have demonstrated a wafer trimming technique which combines two successive rounds of design, fabrication, and measurement together to produce a final resonator array with ideal frequency spacing and extremely low frequency collision rate. We use this technique on a 127-resonator array made from a TiN/Ti/TiN multilayer film and show that the array yield improves from 84% to 97%, while the resonator quality factors and noise properties remain unaffected. We have also demonstrated that the measured resonance frequency matches its design

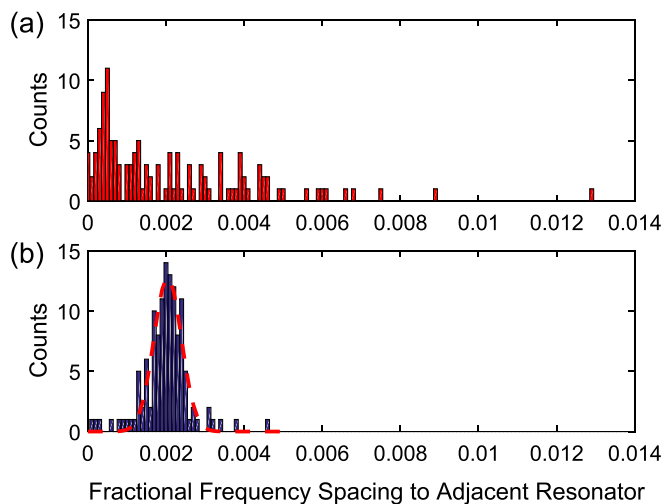


FIG. 4. (a) Histogram of the fractional frequency spacing before the trimming process. (b) Histogram of the fractional frequency spacing after the trimming process. The red dash line fits to a Gaussian distribution $f(x) = \frac{1}{\sqrt{2\pi}\sigma} e^{-\frac{(x-\mu)^2}{2\sigma^2}}$, with $\mu = 0.002$ and $\sigma = 3.5 \times 10^{-4}$.

value within an accuracy of 4.5×10^{-3} after the trimming process.

The proposed wafer trimming technique and its principle are applicable to any superconducting films, even films with poor uniformity, and other resonator types than lumped-element resonators. It can also be easily modified to re-adjust other parameters of the array (such as the coupling Q_c). Our technique provides an easy-to-implement and effective tool to improve the yield and multiplexing density of large resonator arrays, which may find broad applications in photon detection and quantum computing.

See [supplementary material](#) for the derivation of frequency collision probability and array yield formula.

The MKID devices were fabricated in the NIST-Boulder microfabrication facility. We thank Professor Xie Dong for his technical assistance. This work was supported in part by the National Natural Science Foundation of China (Grant Nos. 61301031 and U1330201). Contribution of the U.S. Government, not subject to copyright.

- ¹P. K. Day, H. G. LeDuc, B. A. Mazin, A. Vayonakis, and J. Zmuidzinas, *Nature* **425**, 817 (2003).
- ²M. A. Castellanos-Beltran, K. D. Irwin, L. R. Vale, G. C. Hilton, and K. W. Lehnert, *IEEE Trans. Appl. Supercond.* **19**, 944 (2009).
- ³A. Blais, R.-S. Huang, A. Wallraff, S. M. Girvin, and R. J. Schoelkopf, *Phys. Rev. A* **69**, 062320 (2004).
- ⁴M. Will, M. Hamer, M. Müller, A. Noury, P. Weber, A. Bachtold, R. V. Gorbachev, C. Stampfer, and J. Güttinger, *Nano Lett.* **17**, 5950–5955 (2017).
- ⁵S. Doyle, P. Mauskopf, J. Naylon, A. Porch, and C. Duncombe, *J. Low Temp. Phys.* **151**, 530 (2008).
- ⁶J. Baselmans, *J. Low Temp. Phys.* **167**, 292 (2012).
- ⁷J. Zmuidzinas, *Annu. Rev. Condens. Matter Phys.* **3**, 169 (2012).
- ⁸J. Baselmans, S. Yates, R. Barends, Y. Lankwarden, J. Gao, H. Hoevers, and T. Klapwijk, *J. Low Temp. Phys.* **151**, 524 (2008).
- ⁹J. Hubmayr, J. Beall, D. Becker, H.-M. Cho, M. Devlin, B. Dober, C. Groppi, G. C. Hilton, K. D. Irwin, D. Li *et al.*, *Appl. Phys. Lett.* **106**, 073505 (2015).
- ¹⁰B. A. Mazin, B. Bumble, S. R. Meeker, K. O'Brien, S. McHugh, and E. Langman, *Opt. Express* **20**, 1503 (2012).
- ¹¹D. Moore, S. Golwala, B. Bumble, B. Cornell, P. Day, H. LeDuc, and J. Zmuidzinas, *Appl. Phys. Lett.* **100**, 232601 (2012).
- ¹²S. Rowe, E. Pascale, S. Doyle, C. Dunscombe, P. Hargrave, A. Papageorgio, K. Wood, P. A. Ade, P. Barry, A. Bideaud *et al.*, *Rev. Sci. Instrum.* **87**, 033105 (2016).
- ¹³J. Gao, M. Vissers, M. Sandberg, F. Da Silva, S. W. Nam, D. Pappas, D. Wisbey, E. Langman, S. Meeker, B. Mazin *et al.*, *Appl. Phys. Lett.* **101**, 142602 (2012).
- ¹⁴W. Guo, X. Liu, Y. Wang, Q. Wei, L. Wei, J. Hubmayr, J. Fowler, J. Ullom, L. Vale, M. Vissers *et al.*, *Appl. Phys. Lett.* **110**, 212601 (2017).
- ¹⁵N. Galitzki, P. A. Ade, F. E. Angilè, P. Ashton, J. A. Beall, D. Becker, K. J. Bradford, G. Che, H.-M. Cho, M. J. Devlin *et al.*, *J. Astron. Instrum.* **3**, 1440001 (2014).
- ¹⁶A. Monfardini, A. Benoit, A. Bideaud, L. Swenson, A. Cruciani, P. Camus, C. Hoffmann, F. Désert, S. Doyle, P. Ade *et al.*, *Astrophys. J., Suppl. Ser.* **194**, 24 (2011).
- ¹⁷J. Sayers, R. P. Duan, S. R. Golwala, M. I. Hollister, A. Lam, D. A. Miller, J. A. Schlaerth, S. R. Siegel, A. Vayonakis, and J. Zmuidzinas, *Proc. SPIE* **9153**, 915304 (2014).
- ¹⁸J. van Eyken, M. Strader, A. Walter, S. Meeker, P. Szypryt, C. Stoughton, K. O'Brien, D. Marsden, N. Rice, Y. Lin *et al.*, *Astrophys. J., Suppl. Ser.* **219**, 14 (2015).
- ¹⁹A. M. Baryshev, J. J. A. Baselmans, S. J. C. Yates, L. Ferrari, L. Bisigello, R. M. J. Janssen, A. Endo, T. M. Klapwijk, B. Klein, S. Heyminck *et al.*, in *2014 39th International Conference on Infrared, Millimeter, and Terahertz Waves (IRMMW-THz)* (2014), pp. 1–1.

- ²⁰S. Shu, M. Calvo, S. Leclercq, J. Goupy, A. Monfardini, and E. Driessen, preprint [arXiv:1710.08232](https://arxiv.org/abs/1710.08232) (2017).
- ²¹M. Velázquez, D. Ferrusca, E. Castillo-Dominguez, E. Ibarra-Medel, S. Ventura, V. Gómez-Rivera, D. Hughes, I. Aretxaga, W. Grant, S. Doyle *et al.*, *J. Low Temp. Phys.* **184**, 799 (2016).
- ²²M. R. Vissers, J. Gao, J. S. Kline, M. Sandberg, M. P. Weides, D. S. Wisbey, and D. P. Pappas, *Thin Solid Films* **548**, 485 (2013).
- ²³M. R. Vissers, J. Gao, M. Sandberg, S. M. Duff, D. S. Wisbey, K. D. Irwin, and D. P. Pappas, *Appl. Phys. Lett.* **102**, 232603 (2013).
- ²⁴B. Mazin, S. R. Meeker, M. Strader, P. Szypryt, D. Marsden, J. van Eyken, G. Duggan, A. Walter, G. Ulbricht, M. Johnson *et al.*, *Publ. Astron. Soc. Pac.* **125**, 1348 (2013).
- ²⁵B. Dober, J. Ausermann, J. Beall, D. Becker, G. Che, H. Cho, M. Devlin, S. Duff, N. Galitzki, J. Gao *et al.*, *J. Low Temp. Phys.* **184**, 173 (2016).
- ²⁶X. Liu, W. Guo, Y. Wang, L. Wei, C. Mckenney, B. Dober, T. Billings, J. Hubmayr, L. Ferreira, M. Vissers *et al.*, *J. Appl. Phys.* **122**, 034502 (2017).
- ²⁷C. M. McKenney, J. Gao, G. Hilton, J. Hubmayr, and M. R. Vissers, “Fabrication method for micro-resonator arrays scalable to arbitrary geometries and optimized for high multiplexing factors” (unpublished).